Optics Letters

# Controlling ultrafast laser writing in silica glass by pulse temporal contrast

Yuhao Lei,[1,3] Huijun Wang,[1] Gholamreza Shayeganrad,[1] Yuri Svirko,[2] and Peter G. Kazansky[1,*]

[1]Optoelectronics Research Centre, University of Southampton, Southampton SO17 1BJ, United Kingdom
[2]Center for Photonics Sciences, University of Eastern Finland, FI-80100 Joensuu, Finland
[3]yuhao.lei@soton.ac.uk
*pgk@soton.ac.uk

Received 26 February 2024; revised 29 March 2024; accepted 29 March 2024; posted 2 April 2024; published 25 April 2024

**We demonstrate that the temporal contrast of femtosecond light pulses is a critical parameter in laser writing inside transparent dielectrics, allowing different material modifications. In particular, anisotropic nanopores in silica glass are produced by high-contrast of $10^7$ femtosecond Yb:KGW laser pulses rather than low-contrast of $10^3$ Yb fiber laser pulses. The difference originates in the fiber laser storing a third of its energy in a post-pulse of up to 200 ps duration. The absorption of this low-intensity fraction of the pulse by laser-induced transient defects with relatively long lifetime and low excitation energy, such as self-trapped holes, drastically changes the kinetics of energy deposition and the type of material modification. We also demonstrate that low-contrast pulses are effective in creating lamellar birefringent structures, possibly driven by a quadrupole nonlinear current.**



https://doi.org/10.1364/OL.522307

The interaction of intense ultrashort light pulses with transparent materials has attracted considerable interest due to its strong application potential. Since the first demonstration three decades ago [1], femtosecond micromachining has found a wide range of applications spanning from eye surgery [2] to fabrication of photonic components [3–5] and optical data storage [6]. Rapid deposition of energy carried by sub-picosecond light pulses into transparent dielectric involves a complex physical phenomena [7], driven by the generation of free electrons in the irradiated volume via multiphoton, tunneling, and avalanche ionization [8]. The free electron may also occur due to multiphoton ionization of self-trapped excitons and other defects, which are formed within the silica glass bandgap [9] and can be detected by using fluorescence, electron spin resonance, and other techniques [10,11]. Inverse Bremsstrahlung absorption in a free electron ensemble leads to irreversible permanent modification of the material [2] due to the energy transfer to the lattice within the electron–phonon relaxation time [12].

Depending on the conditions, permanent modification of the silica glass under irradiation with femtosecond optical pulses manifests itself as the refractive index increase (often referred as type 1 modification) [3], form birefringence created by sub-wavelength spaces nanoplatelets or nanogratings (type 2) [13], flattened nanopores (type X) [14], and voids (type 3) [6]. Nanostructured silica glass has been used for selective etching [4], polarization beam shaping [5], and five-dimensional (5D) optical data storage [15].

One of the main parameters that determine the type of material modification is the pulse duration; e.g., pulse energy threshold for formation of the birefringent structures increases with decreasing pulse duration from 200 to 40 fs, which correlates with the self-trapping of excitons in silica glass at 250 fs [16]. More recently it has been demonstrated that in silicon, the material modification depends not only on the pulse duration but also on the pulse contrast. Specifically, it has been observed that at the same peak intensity, the femtosecond pulses generated by fiber lasers increase the refraction index of silicon in the irradiated volume [17], while pulses from an optical parametric amplifier (OPA) pumped by a Ti:Sapphire laser [18,19] do not. Such a difference has been explained by the fact that the temporal contrasts of light pulses produced by these laser systems [20] are different with a fiber laser typically generating femtosecond pulses having subnanosecond pedestal comparable with lifetime of free electrons in silicon [21]. The pico- or subnanosecond pedestal of the fiber laser pulse is sufficient for the modification of silicon via two-photon absorption, while a pedestal-free OPA pulse of the same intensity is unable to do so because its energy is too low. However, there was a common belief that this pedestal is irrelevant for laser writing inside transparent dielectrics, in which the underlying modification mechanism relies on multiphoton (eight-photon at 1030 nm wavelength for fused silica) absorption that requires light intensities achievable only with tightly focused femtosecond laser pulses.

Here we demonstrate that the subnanosecond pedestal can also drastically affect the writing ability of a femtosecond laser pulse in silica glass. We show that a fiber laser operating at sub-MHz repetition rate is not suitable for the formation of

birefringent nanopore structures (type X modification) in silica glass; however, it can be used to produce highly birefringent lamella-shaped voxels (type 2m modification). In contrast, the Yb:KGW laser can write anisotropic structures with flattened nanopores (type X) or isotropic modifications with an increased refractive index (type 1) in a wider range of parameters. The pulse contrast measurements reveal a correlation between the micromachining performance and presence of the subnanosecond pedestal in the femtosecond laser pulse. Our analysis shows that the energy stored in the pulse pedestal is also transferred into the irradiated volume despite its low intensity via absorption by defects created in the irradiated volume by the femtosecond pulse. These defects such as self-trapped holes (STHs) possess a low excitation potential enabling the deposition of the pedestal energy into an irradiated volume and, correspondingly, affecting the writing performance.

The writing experiments were carried out with two laser systems operating the same wavelength of 1030 nm. The first one is a mode-locked regeneratively amplified Yb-doped potassium gadolinium tungstate (Yb:KGW) laser (Pharos, Light Conversion Ltd.). The second system is a Yb-doped fiber laser (Satsuma, Amplitude Systems). The Satsuma laser beam was expanded by a telescope system to match the Pharos laser beam diameter. The energy of the laser pulses was controlled by an external attenuator. For both setups, we maintained identical parameters for the pulse duration ($\tau$), repetition rate (RR), and pulse energy ($E_p$), which were varied within the ranges of 270–500 fs for $\tau$, 100 kHz to 1 MHz for RR, and 450 nJ to 1 μJ for $E_p$.

The temporal contrast of the laser pulse was measured by a high dynamic range autocorrelator (pulseCheck SM Type 2, APE). The laser beam was focused via a 0.16 or 0.4 NA aspheric lens 170 μm below the surface of a synthetic silica glass substrate, which was mounted on an XYZ linear air-bearing translation stage (Aerotech Ltd.). The retardance and slow axis azimuth of laser-induced modifications were analyzed with an Olympus BX51 optical microscope equipped with a birefringence measurement system (CRi Abrio imaging system) operating at 546 nm wavelength.

Both lasers were used to imprint voxels at RR = 500 kHz, $\tau$ = 300 fs, $E_p$ = 700 nJ, NA = 0.16, and scan speed of 1 mm/s, while the translation stage moved horizontally. Figure 1 shows the visualized birefringence written with different numbers of pulses ($N_p$) using both laser systems. One can observe from Fig. 1(a) that when writing with the Yb:KGW laser, no noticeable induced birefringence was observed at $N_p < 20$, while at $20 < N_p < 150$, type X birefringent voxels, which are not seen in the transmittance, were observed. At $N_p > 150$, birefringent voxels begin to appear in transmission, which indicates an increase in the size and their clustering, and randomly distributed nanolamella formed (type X-2). When the number of pulses exceeds 400, lamella-like birefringent structures oriented perpendicular to the plane of polarization of the laser beam appear on birefringent and optical images, associated with type 2m modification. When the laser pulse energy was increased up to 800 nJ at $N_p > 500$, we observed periodic visible lamella-shaped structures (type 2m) separated by $\lambda/n \approx 700$–800 nm [Fig. 1(b)], where $\lambda$ = 1030 nm is the excitation wavelength, and n = 1.45 is the refractive index of the silica glass. It is worth noting that such lamella-shaped structures with period of $\lambda/n$ were previously observed only in SEM images of imprinted modifications [22,23]. A table was used to compare laser-induced different birefringent modifications in silica glass, as shown in Table S1, Supplement 1.

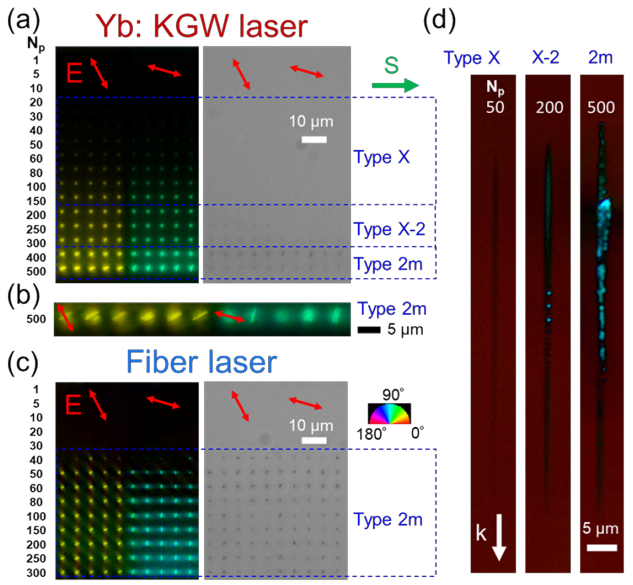


**Fig. 1.** Birefringence and optical images of laser written voxels. Top view of birefringent voxels written by (a) and (b) Yb:KGW laser, and (c) fiber laser. Birefringence image (left) and corresponding optical transmission image (right) of imprinted voxels were captured. (d) Side view birefringence image of different voxels. The red arrow shows polarization of the laser beam, and pseudo-colors (inset) indicate the local orientation of the slow axis. The green (white) arrow presents the scanning (beam propagation) direction. Processing conditions for (a) and (c): 1030 nm wavelength, 300 fs pulse duration, 700 nJ pulse energy, 500 kHz repetition rate, 1–500 number of pulses ($N_p$), focusing via 0.16 NA lens. $E_p$ = 800 nJ in (b) and (d).

Surprisingly, no "optically invisible" birefringent voxels (type X) were written by using the fiber laser with the same parameters. One can observe from Fig. 1(c) that no modification has been observed at $N_p < 40$, while at $40 < N_p < 300$, birefringent lamella-shaped voxels (type 2m), which are seen both in the birefringence and optical transmission, were imprinted [Fig. 1(c)].

By writing with the Yb:KGW laser, the slow axis of birefringent voxels was always perpendicular to the polarization azimuth of the writing laser beam (Fig. S1, Supplement 1). Figure 1(d) shows modifications (type X at $N_p$ = 50, type X-2 at $N_p$ = 200 and type 2m at $N_p$ = 500) along the beam propagation axis where the writing laser beam propagates from the top to the bottom in the image. The 57 μm long modified area is uniform and comprises randomly arranged anisotropic nanopores (type X) [Fig. 1(d), left]. On the contrary, at $N_p$ = 200, type X-2 modification with a length of 65 μm comprises birefringent dot-shaped structures in the middle of the modified area [Fig. 1(d), middle]. At $N_p$ = 500, lamella-shaped type 2m modifications are observed at the upper part of the modified area [Fig. 1(d), right]. Moreover, lamellae with the wavelength periodicity were also observed in a birefringent square written by raster scanning with a 1 μm line separation (Fig. S2, Supplement 1).

Figure 2 shows the retardance of birefringent voxels written by using Yb:KGW and fiber lasers. At the pulse energy of 700 nJ, Yb:KGW laser pulses produced type X voxels at $N_p \leq 150$ and type X-2 voxels at $200 < N_p < 300$ [Fig. 2(a)]. The later finding is

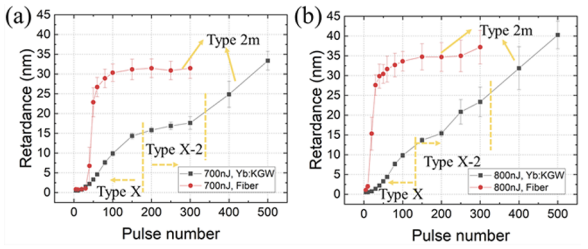


**Fig. 2.** Retardance of birefringent voxels versus writing pulse number for two lasers. (a) Pulse energy of 700 nJ and (b) 800 nJ. Processing conditions: $\lambda = 1030$ nm, $\tau = 300$ fs, RR = 500 kHz, 0.16 NA lens.

consistent with previously reported results [24]. In contrast, the fiber laser produces type 2m modification (i.e., lamella-shaped structures), in which the retardance rapidly increases with the number of pulses and saturates at $N_p \approx 100$. At $N_p = 200$, the retardance $Ret = \Delta n_b l$, where $\Delta n_b$ and $l$ are birefringence and length of the modified area, respectively, of type 2m voxels written by the fiber laser is about two times higher than that of type X-2 voxels imprinted by the Yb:KGW laser with the same parameters. The retardances of type 2m voxels written with Yb:KGW or fiber lasers are similar, which is about 33 (31) nm for 500 (300) pulses from the Yb:KGW (fiber) laser at $E_p = 700$ nJ. Given by voxel length $l = 65$ μm, one can estimate the birefringence for voxels written with 200 pulses of the fiber and Yb:KGW lasers is $4.9 \times 10^{-4}$ (type 2m) and $2.3 \times 10^{-4}$(type X-2) respectively. A similar trend was observed at writing pulse energy of 800 nJ [Fig. 2(b)].

To further elucidate the difference in the parameter windows for obtaining the type X modification, experiments were carried out using different repetition rates, pulse numbers, energies, and durations for both lasers. While the type X modification was produced with a Yb:KGW laser at the pulse duration of 300 fs and a RR of 500 kHz in the pulse energy range from 450 to 900 nJ [Fig. 3(a)], the fiber laser was unable to produce any detectable modifications at a pulse energy of less than 700 nJ at the same RR and pulse duration [Fig. 3(b)]. That is, one can conclude that since the modification threshold for the fiber laser is about 1.5 times larger than that of the Yb:KGW laser, one may expect that the actual fiber laser intensity is lower than that of the Yb:KGW laser. However, at the pulse energy above 700 nJ, the fiber laser pulses produce lamella-shaped voxels having stronger birefringence in comparison with the obtained by the Yb:KGW laser.

On the other hand, at RR = 1 MHz and $E_p = 500$ nJ, type X voxels can be created by the fiber laser; however in a narrower—compared to the Yb:KGW laser—pulse energy range (Fig. S3a, Supplement 1). At a longer pulse duration of 500 fs and RR = 500 kHz, the type X modification was observed in the pulse energy range from 550 nJ to 1 μJ for the Yb:KGW laser and was not observed with the fiber laser (Fig. S3b, Supplement 1). At RR = 1 MHz and $\tau = 500$ fs, the parameter window for the type X formation with the fiber laser should be narrow—similarly to the 300 fs long pulses—than that for Yb:KGW laser (Fig. S3c, Supplement 1).

The difference between the characteristics of the fiber laser at RR = 500 kHz and RR = 1 MHz can be explained by the accumulation of third-order nonlinear effects in the fiber amplifier chain, e.g., self-phase modulation, produced with greater efficiency by

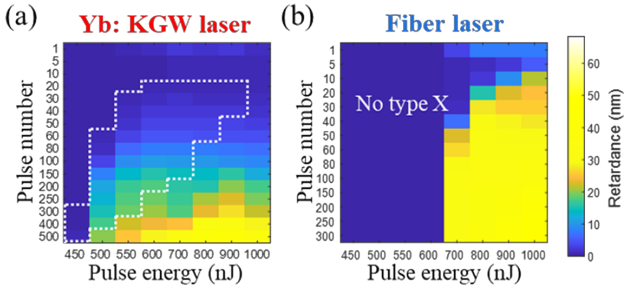


**Fig. 3.** Dependence of retardance on laser parameters. (a) and (b) Retardance maps as functions of pulse energy and pulse number for Yb:KGW laser (left) and fiber laser (right) with pulse duration of 300 fs and repetition rates of 500 kHz. The areas within white dotted lines show the type X modification region.

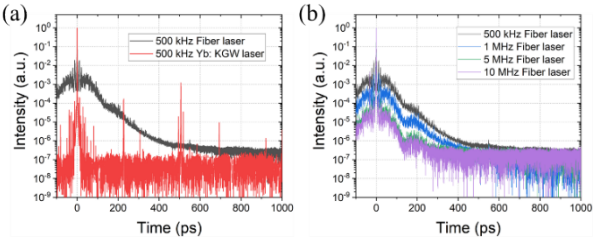


**Fig. 4.** Temporal contrast ratio of 300 fs pulses from Yb:KGW and fiber lasers over a time range of −100 to 1000 ps. (a) Comparison of the contrast ratio at a repetition rate of 500 kHz for both lasers. (b) Contrast ratio for fiber laser at various repetition rates.

ultrashort light pulses with a higher intensity at RR = 500 kHz, leading to the formation of a subnanosecond pedestal.

To verify this hypothesis, we characterized the temporal contrast of pulses from two lasers by an autocorrelator having the maximum dynamic range of $10^7$. At a repetition rate of 500 kHz, the temporal contrast of pulses from the Yb:KGW laser was around $10^7$, i.e., produced pulses have no noticeable pedestal [Fig. 4(a)]. On the contrary, at RR = 500 kHz, the temporal contrast of the fiber laser pulses was as low as $10^3$, i.e., at the pulse duration of 300 fs and the pedestal width of about 200 ps, the pedestal carries nearly 32% of the pulse energy. Correspondingly, at the pulse energy of 700 nJ, the peak powers for the femto- and subnanosecond components of the pulse are 1.6 MW and 1.1 kW, respectively. Thus, the actual intensity of focused femtosecond pulses produced by Yb:KGW and the fiber lasers is 10 and 6.8 TW/cm$^2$, respectively. The latter explains why the threshold pulse energy required for the material modification with the fiber laser is 1.5 times higher than that of the Yb:KGW laser. Moreover, the parameter window for the isotropic refractive index increase is also broader for high-contrast pulses (Fig. S4, Supplement 1). The autocorrelation trace cannot distinguish between pre- and post-pulse; however, given the nonlinear nature of pedestal formation, it is more likely to be associated with a post-pulse.

We also compared the temporal contrast of the fiber laser pulses at repetition rates of 500 kHz, 1 MHz, 5 MHz, and 10 MHz. One can observe from Fig. 4(b) that the higher the RR, the better the temporal contrast because increasing the repetition rate results in the suppression of the self-phase modulation of the low peak power pulse in the fiber laser amplifier chain. However, even at RR = 10 MHz the achievable contrast of $10^5$ is

still two orders lower than that observed for the Yb:KGW laser at RR = 500 kHz. The temporal contrast can be improved by using appropriate phase compensation techniques.

Lamella-shaped birefringent (type 2m) modification, which is stronger and observed at a lower threshold for fiber laser, may originate from the absorption of the subnanosecond pedestal that carries about a third of the pulse energy. Since the lifetime of free electrons in silica glass is less than 1 ps [25,26], one can expect the existence of an alternative light absorption channel. We believe that the key role is played by self-trapped holes (STHs) [27,28], which have a short lifetime at room temperature and low excitation energy (1–2 eV) [29]. Created in the irradiated volume by femtosecond portion (68% in energy) of the fiber laser pulse, they are capable of absorbing a significant part of the pulse pedestal energy due to one- and two-photon absorption, promoting the formation of lamella-shaped structures rather than nanopores in the irradiated volume.

One may also suggest that the nonlinear current defined by the concentration gradient and light polarization, which reads $\boldsymbol{j}_q \propto (\nabla n\boldsymbol{E})\boldsymbol{E}$ [30,31], where $n$ is the concentration of charge carriers, and $\mathbf{E}$ is the electric field of the light beam, participates in the formation of lamella-shaped structures oriented perpendicular to the polarization and possibly plays a key role in nanograting formation.

Indeed, this nonlinear current is an analog of the quadrupole nonlinear polarization, which is responsible, e.g., for the generation of the second harmonic in an isotropic medium. Interestingly, this nonlinear current, determined by the polarization of the light beam, is also directed against the charge concentration gradient, which leads to its amplification. The latter can explain the creation of narrow lamella-like structures oriented perpendicular to the direction of light polarization. Moreover, the evanescent near-field component along the polarization direction created by lamella-like nanostructures propagates with a speed of light along the polarization and can interfere with the incident light field [32]. Such an interference results in the spatial modulation of the light intensity and concentration of light-induced defects, e.g., self-trapped holes with a wavelength periodicity along the direction of polarization. Earlier, the mechanism of formation of structures with a periodicity of the wavelength was also discussed [33].

In conclusion, we demonstrate that in transparent materials, the material modification is governed not only by the pulse duration and energy, but also by the pulse contrast. The important consequence of our experimental finding is that the interpretation of data published over the past two decades on micromachining in transparent materials with fiber lasers may require revision [34]. The pedestal of fiber laser pulses can be reduced by using its second harmonic or running at a higher RR. Efficient formation of lamella-shaped birefringent structures (type 2m) with larger birefringence can be attributed to the absorption of low power subnanosecond pulse pedestal by transient defects with low excitation energy, such as self-trapped holes, produced by high-power femtosecond part of the pulse [28]. Such lamella-like structures can be beneficial for applications in etching-assisted micromachining of silica glass [4]. Periodic structures with wavelength periodicity indicate that the material modification mechanism, involving the interference of incident light with the evanescent near-field component created by the nanostructure, is an alternative to the interference of the incident and the inhomogeneity-scattered light waves.

**Funding.** European Research Council (ENIGMA, 789116); Microsoft (Project Silica); H2020 Marie Skłodowska-Curie Actions (CHARTIST, 101007896); Research Council of Finland (320166, 343393, Flagship Program PREIN).

**Acknowledgment.** The authors acknowledge Mateusz Ibek from APE GmbH for lending us the high dynamic range autocorrelator. We acknowledge Clemens Hoenninger from Amplitude and Martynas Baskauskas from Light Conversion for useful discussions.

**Disclosures.** The authors declare no conflicts of interest.

**Data availability.** Data underlying the results presented in this paper are not publicly available at this time but may be obtained from the authors upon reasonable request.

**Supplemental document.** See Supplement 1 for supporting content.

## REFERENCES

1. P. Pronko, S. Dutta, J. Squier, *et al.*, Opt. Commun. **114**, 106 (1995).
2. A. Vogel, J. Noack, G. Hüttman, *et al.*, Appl. Phys. B **81**, 1015 (2005).
3. K. M. Davis, K. Miura, N. Sugimoto, *et al.*, Opt. Lett. **21**, 1729 (1996).
4. Y. Bellouard, A. Said, M. Dugan, *et al.*, Opt. Express **12**, 2120 (2004).
5. M. Beresna, M. Gecevičius, P. G. Kazansky, *et al.*, Appl. Phys. Lett. **98**, 201101 (2011).
6. E. Glezer, M. Milosavljevic, L. Huang, *et al.*, Opt. Lett. **21**, 2023 (1996).
7. B. Stuart, M. Feit, A. Rubenchik, *et al.*, Phys. Rev. Lett. **74**, 2248 (1995).
8. C. B. Schaffer, A. Brodeur, and E. Mazur, Meas. Sci. Technol. **12**, 1784 (2001).
9. S. Mao, F. Quéré, S. Guizard, *et al.*, Appl. Phys. A **79**, 1695 (2004).
10. L. Skuja, M. Hirano, H. Hosono, *et al.*, Phys. Status Solidi C **2**, 15 (2005).
11. R. Stoian, K. Mishchik, G. Cheng, *et al.*, Opt. Mater. Express **3**, 1755 (2013).
12. R. R. Gattass and E. Mazur, Nat. Photonics **2**, 219 (2008).
13. Y. Shimotsuma, P. G. Kazansky, J. Qiu, *et al.*, Phys. Rev. Lett. **91**, 247405 (2003).
14. M. Sakakura, Y. Lei, L. Wang, *et al.*, Light: Sci. Appl. **9**, 15 (2020).
15. J. Zhang, M. Gecevicius, M. Beresna, *et al.*, Phys. Rev. Lett. **112**, 033901 (2014).
16. C. Hnatovsky, R. S. Taylor, P. P. Rajeev, *et al.*, Appl. Phys. Lett. **87**, 014104 (2005).
17. I. Pavlov, O. Tokel, S. Pavlova, *et al.*, Opt. Lett. **42**, 3028 (2017).
18. A. Mouskeftaras, A. V. Rode, R. Clady, *et al.*, Appl. Phys. Lett. **105**, 191103 (2014).
19. M. Chanal, V. Y. Fedorov, M. Chambonneau, *et al.*, Nat. Commun. **8**, 773 (2017).
20. A. Wang, A. Das, and D. Grojo, Phys. Rev. Res. **2**, 033023 (2020).
21. A. Mouskeftaras, M. Chanal, M. Chambonneau, *et al.*, Appl. Phys. Lett. **108**, 041107 (2016).
22. J. Wang, X. Liu, Y. Dai, *et al.*, Opt. Express **26**, 12761 (2018).
23. F. Zimmermann, S. Richter, R. Buschlinger, *et al.*, in *Optically Induced Nanostructures: Biomedical and Technical Applications* (De Gruyter, 2015), Chap. 5.
24. H. Wang, Y. Lei, L. Wang, *et al.*, Laser Photonics Rev. **16**, 2100563 (2022).
25. P. Audebert, P. Daguzan, A. Dos Santos, *et al.*, Phys. Rev. Lett. **73**, 1990 (1994).
26. Q. Sun, H. Jiang, Y. Liu, *et al.*, Opt. Lett. **30**, 320 (2005).
27. D. L. Griscom, Phys. Rev. B **40**, 4224 (1989).
28. Y. Lei, H. Wang, L. Skuja, *et al.*, Laser Photonics Rev. **17**, 2200978 (2023).
29. P. F. Kashaykin, A. L. Tomashuk, M. Y. Salgansky, *et al.*, J. Appl. Phys. **121**, 213104 (2017).
30. E. M. Dianov, P. Kazanskiĭ, and D. Y. Stepanov, Sov. J. Quantum Electron. **19**, 575 (1989).
31. D. Z. Anderson, V. Mizrahi, and J. E. Sipe, Opt. Lett. **16**, 796 (1991).
32. P. Temple and M. Soileau, IEEE J. Quantum Electron. **17**, 2067 (1981).
33. A. Rudenko, J.-P. Colombier, and T. E. Itina, Phys. Rev. B **93**, 075427 (2016).
34. K. Sugioka and Y. Cheng, Light: Sci. Appl. **3**, e149 (2014).